

Differential Binding of Rimantadine Enantiomers to Influenza A M2 Proton Channel

Anna K. Wright,^{†,‡} Paratchata Batsomboon,[§] Jian Dai,^{†,#} Ivan Hung,[‡] Huan-Xiang Zhou,^{†,#} Gregory B. Dudley,^{†,§} and Timothy A. Cross^{*,†,‡,§}

[†]Institute of Molecular Biophysics, [§]Department of Chemistry and Biochemistry, and [#]Department of Physics, Florida State University, Tallahassee, Florida 32306, United States

[‡]National High Magnetic Field Laboratory, Florida State University, Tallahassee, Florida 32310, United States

S Supporting Information

ABSTRACT: Rimantadine hydrochloride (α -methyl-1-adamantane-methylamine hydrochloride) is a chiral compound which exerts antiviral activity against the influenza A virus by inhibiting proton conductance of the M2 ion channel. In complex with M2, rimantadine has always been characterized as a racemic mixture. Here, we report the novel enantioselective synthesis of deuterium-labeled (*R*)- and (*S*)-rimantadine and the characterization of their protein–ligand interactions using solid-state NMR. Isotropic chemical shift changes strongly support differential binding of the enantiomers to the proton channel. Position restrained simulations satisfying distance restraints from ¹³C–²H rotational-echo double-resonance NMR show marked differences in the hydrogen-bonding pattern of the two enantiomers at the binding site. Together these results suggest a complex set of interactions between (*R*)-rimantadine and the M2 proton channel, leading to a higher stability for this enantiomer of the drug in the channel pore.

For several decades the Food and Drug Administration has recommended the characterization of pure enantiomers, due to the structural differences in chiral compounds, which lead to variability in pharmacological properties and mode of action at the target site.¹ Antiviral activity and protein–ligand interactions of rimantadine hydrochloride (α -methyl-1-adamantane-methylamine hydrochloride), in complex with the M2 proton channel from influenza A virus, have always been evaluated using a racemic mixture of the drug. Here, the separate enantiomers of rimantadine as well as the racemic mixture are experimentally investigated. The prevalence of drug-resistant viral strains has halted clinical use of this inhibitor due to loss of therapeutic efficacy. Nonetheless, there is ongoing interest in characterizing the structural basis for rimantadine action at the atomic level to aid in the design of novel inhibitors. Recent experimental investigations of the truncated M2 channel in complex with rimantadine have provided some insight into stabilizing interactions at the binding site.² Characterizing protein–ligand interactions for each enantiomer separately will identify potential stereospecific rimantadine binding interactions to the M2 proton channel. In addition, characterizing the relative binding affinity for each enantiomer can suggest potential differences in pharmacological

properties. For instance, the binding of *L*-tryptophan to albumin is 100 times greater than for *D*-tryptophan.³

The target of rimantadine, the M2 integral membrane protein, functions at multiple stages of the influenza A viral life cycle and is essential for viral replication.⁴ Truncated constructs of M2, its transmembrane domain (M2TM, residues ~22–46) and its conductance domain (M2CD, residues ~22–62) have been the subject of numerous structural characterization efforts.^{5–10} In light of its pharmacological relevance, a number of investigations have also focused on characterizing structural changes induced by drug binding. Both of the previously licensed anti-influenza inhibitors of the M2 channel, amantadine and rimantadine, have been evaluated.^{5,11–13} While it has been established that proton conductance by the homotetrameric M2 proton channel across the viral membrane is inhibited by these adamantane analogues, the mechanistic details of inhibition still remain unclear.^{13–15}

A number of important observations with regard to drug binding were reported by the aforementioned studies. Two binding sites were initially observed. The lipid facing site at D44 exists when M2 is solubilized in a detergent environment or under high inhibitor concentration when M2TM is solubilized in lipid bilayers.^{6,7,13} The pore localized binding pocket in the N-terminal region has been shown to be the primary binding site in both M2TM and M2CD.^{2,7,9,11,12,15} Not surprisingly, this is also the region of persistent amino acid mutations, L26F, V27A, A30T and S31N, which occur naturally irrespective of amantadine exposure.¹⁶ Most recently, a large-scale sequencing analysis of globally circulating viral strains has shown a prevalence rate of 95% for the S31N mutation.¹⁷ Rimantadine binding to the M2 channel *in vitro* can be monitored through chemical shift observation of this residue using solid state NMR (ssNMR) experiments. In the presence of rimantadine the Ser31 site in M2CD of the wild-type channel undergoes a significant isotropic ¹⁵N chemical shift perturbation of >5 ppm.¹³

In addition to identifying the primary drug binding site, several protein–ligand interactions have been proposed. Early M2/drug models suggested that the polar amine moiety of rimantadine is located in the vicinity of the Ser31 hydroxyl group.^{18a,b} Molecular dynamics (MD) simulations suggested

Received: December 15, 2015

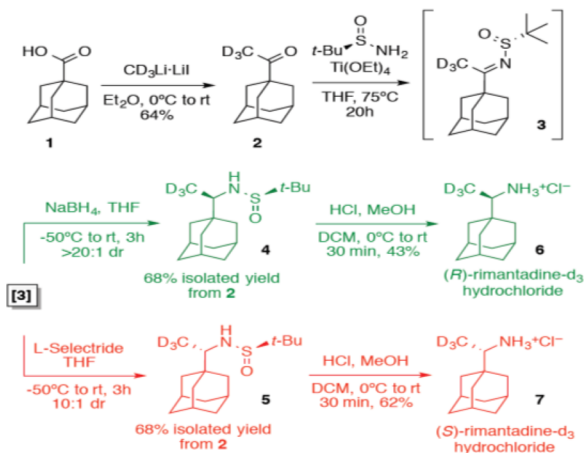
Published: January 25, 2016

that amantadine is oriented with amine toward the channel C-terminus.¹⁹ A rotational-echo double-resonance (REDOR) experiment on the drug-bound M2TM confirmed this orientation.¹² In this investigation, Cady et al. observed a dipolar interaction between the deuterated methyl group of rimantadine and the C α site of Gly34. Static deuterium experiments showed a small time-averaged tilt angle of 13° for rimantadine relative to the channel axis,¹² and a recent study by Griffin et al. provides evidence for a hydrogen bond between the polar amine group and the carbonyl oxygen of Ala30.²

Together these findings suggest that the stability of rimantadine in the channel pore is attained through several noncovalent interactions. However, since rimantadine has previously only been prepared and evaluated as a racemate, it is not possible to determine which interactions are essential and should be used for optimization in structure-based drug design. Considering the near four-fold symmetry of the binding channel and drug dynamics in the channel pore, it is not unreasonable to expect that both enantiomers of rimantadine might bind similarly. Indeed, amantadine is achiral, and it is thought that amantadine and rimantadine bind similarly within the same pocket. However, higher affinity for racemic rimantadine than that of amantadine has been documented.²⁰ Analysis of rimantadine binding as a racemate only provides data on the mix of two potentially different sets of interactions. Here we resolve these two different sets of interactions by analyzing enantiomerically pure rimantadine.

We first set out to prepare the two enantiomers of deuterium-labeled rimantadine (Scheme 1). Enantioselective

Scheme 1. Enantiodivergent Syntheses of (*R*)- and (*S*)-Rimantadine-d₃ Hydrochloride



synthesis of rimantadine has not been reported, so one was developed. Ellman's chiral sulfinamide methodology²¹ proved convenient for this task, as it enabled an enantiodivergent synthetic approach to either enantiomer from a common imine precursor (i.e., 3). Adamantanecarboxylic acid (1) was treated with excess methylolithium-d₃ to produce adamantanyl methyl ketone-d₃ 2, which was condensed with *N*-*tert*-butanesulfinamide in the presence of titanium tetraethoxide to give *N*-*tert*-butanesulfinimide 3. This imide intermediate was not isolated, but instead was treated with either sodium borohydride or *L*-Selectride to give *R_s*, *R* and *R_s*, *S* sulfinamides 4 and 5, respectively, with excellent diastereocontrol in both instances. Solvolysis of the two sulfinamides was accomplished in acidic methanol to produce both (*R*)-rimantadine-d₃ hydrochloride

(6) and (*S*)-rimantadine-d₃ hydrochloride (7) as white solids. This route is expected to be amenable to production of this and other enantiomerically enriched rimantadine isotopomers and analogues.

To evaluate drug binding differences in vitro, we tested each enantiomer in complex with the full length M2 (M2FL) channel. There are 13 serine residues in M2FL. Of these, six are in the N-terminus, one each in the TM and amphipathic helices and five in the C-terminus. Due to spectral overlap, dynamics, and ambiguity in resonance assignments, previous investigations have focused on the shorter M2 channel constructs. Previously, the Ser31 ¹⁵N/¹³C α chemical shifts were reported for M2CD in DOPC/DOPE bilayers as 113.9/63.2 ppm,¹⁰ and separate preparations in DPhPC and POPC lipids had very similar chemical shifts.¹³ To confirm the assignment of the Ser31 resonances from the apo WT preparation, a spectrum of the S31N M2FL mutant is shown in Figure 1A (black) where it

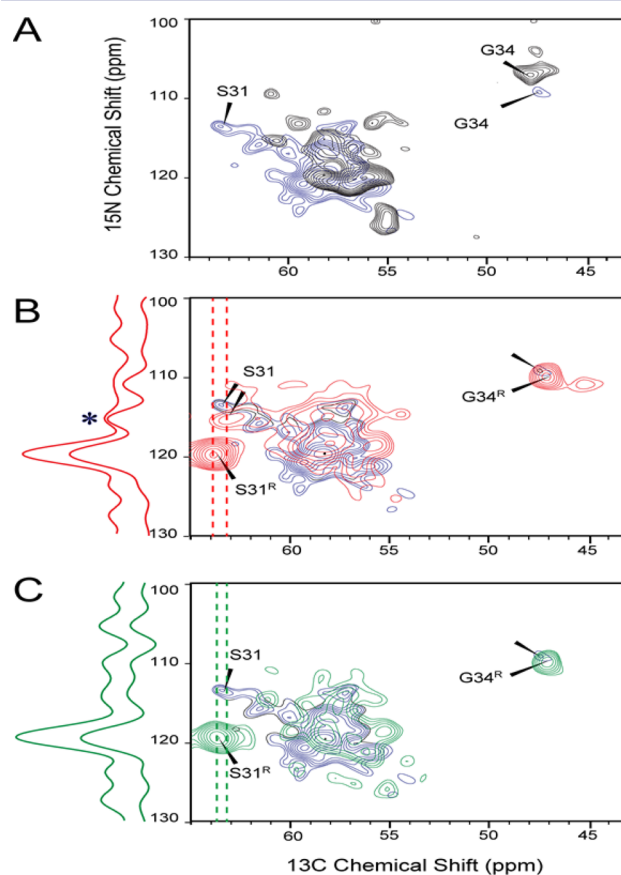


Figure 1. Superimposed 2D ssNMR ¹⁵N/¹³C (NCA) correlation spectra. (A) ¹³C,¹⁵N-Ser,Gly-labeled S31N M2 (black) and WT (blue) channel in the absence of drug. (B) Comparison of WT M2 with (red) and without (blue) bound (*S*)-rimantadine. (C) Comparison of WT M2 with (green) and without bound (*R*)-rimantadine (blue). Drug was added to the sample at 8 drug molecules per channel. Extracted slices are shown from the 2D NCA spectra (¹³C frequencies of 63.9 (B), 63.7 (C), and 63.2 (B, C) ppm).

is seen that the resonance at 113.9/63.2 ppm is absent. The Ser31 ¹⁵N chemical shift changes by ~7 ppm upon binding amantadine.¹³ Consequently, we performed ¹⁵N/¹³C α (NCA) experiments on the M2FL channel in the absence (blue) and presence of the two rimantadine enantiomers (green (*R*) and red (*S*)), in DMPC/DMPG (4:1 molar ratio) lipid bilayers at a

ratio of 1:30 and pH 7.5 (Figure 1B,C). All serine sites, except Ser50 in M2FL are likely to be in weakly or unstructured regions of the protein, as suggested by their weak signal intensity between 55 and 60 ppm in the ^{13}C dimension. All of these sites including Ser50 are likely to have weak intensity due to significant dynamics in the terminal domains of the protein.

In the presence of (*S*)- and (*R*)-rimantadine (Figure 1B,C) a new resonance is observed at 120/64 ppm that is consistent with the study of the racemic mixture of rimantadine, where Andreas et al.¹³ assigned this to the drug bound Ser31 site. This resonance is significantly more intense than the signals for the other 12 serine sites and in comparison to the unbound Ser31 resonance. Interestingly, the Gly34 resonance also appears to be more intense. Such cross-polarization efficiency suggests a more rigid structure for the bound state as previously observed from M2TM studies upon drug binding.⁵

For the (*S*)-rimantadine enantiomer an additional resonance is observed at 115/63 ppm close to the frequencies of the unbound state and potentially in exchange with the bound state. Quantification of this peak is difficult due to the likelihood of more efficient relaxation as in the absence of the drug. Despite the same 1:8 molar ratio of channel to drug for both enantiomers, the data suggest weaker binding of the (*S*)-rimantadine enantiomer in the channel. Unlike the S31N spectrum that shows a significant shift and strengthening of the Gly34 ^{15}N resonance, the binding of rimantadine results in a much more modest shift in the Gly34 ^{15}N and ^{13}C frequencies. The similar frequencies for the Ser31 and Gly34 in the presence of (*S*)- and (*R*)-rimantadine suggest that the binding site and orientation of the drug in the pore are similar for the two enantiomers. In addition, both enantiomers significantly enhance the Ser31 spectral intensity suggesting strong interactions with the drug reduce the backbone dynamics and lead to efficient cross-polarization. To further investigate protein–ligand interactions leading to differences in binding dynamics and conformational geometries, we pursued computational modeling of the enantiomers in complex with M2.

REDOR measurements between methyl-deuterated (*R*)-rimantadine and Gly34 $^{13}\text{C}\alpha$ (Figure 2) in WT M2FL yields a time-averaged distance of 4.5 Å, very similar to that previously determined using M2CD.² The significant reduction in S/S_0 intensity and the observation of a single Gly34 $^{13}\text{C}\alpha$ chemical shift demonstrate that the drug is sampling multiple conformations that are pseudosymmetric or symmetric resulting in a time-averaged distance. With these data for (*R*)-rimantadine and the $^{15}\text{N}/^{13}\text{C}\alpha$ chemical shifts for the Gly34 and Ser31 resonances, the ethylamine of both (*R*)- and (*S*)-rimantadine can be localized to this region of the pore as shown in Figure 3.

RosettaLigand²² was used to dock the enantiomers in the M2 channel by employing REDOR distance restraints. The top ranking poses of (*R*)- and (*S*)-rimantadine were used to prepare position restrained MD simulations of drug-bound M2CD in the same hydrated DMPC/DMPG lipid bilayer environment as in the ssNMR experiments. These simulations showed marked differences in the hydrogen-bonding pattern for the two enantiomers. A plot of these results is shown in Figure 4, where the percentage of simulation frames that show direct and water-mediated hydrogen bonds for both enantiomers is displayed. A higher percentage of the frames having both hydrogen bonding forms is observed for the (*R*)-enantiomer. Snapshots from these simulations are shown in

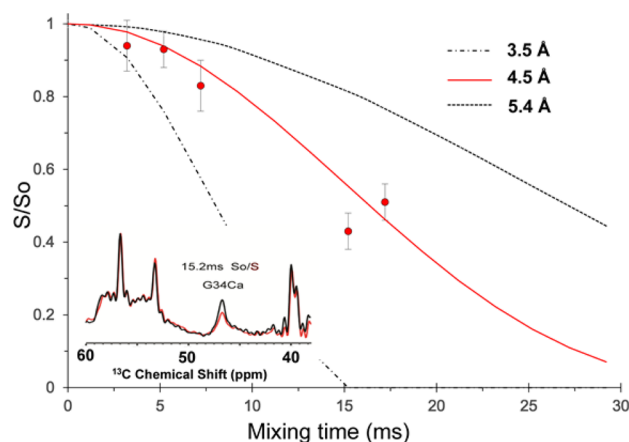


Figure 2. ^{13}C - ^2H REDOR data from M2FL G34Ca in DMPC/DMPG, $S/S_0 = 0.55 \pm 0.05$ at 15.2 ms. Intensity difference between the control S_0 (black) and dephased spectrum S (red) shown as overlay (inset). Drug-channel distance quantification in M2FL: ^{13}C - ^2H REDOR dephasing (S/S_0) as a function of dipolar evolution time for ^{13}C -Ser, Gly WT M2FL in DMPC/DMPG lipid bilayers in complex with (*R*)-rimantadine. Calculated dephasing for a sum of distances contributing to the total dephasing curve (solid red line) fitted to the experimental data points (solid red circles). Error bars are $\pm 2\sigma$. Simulated (S/S_0) trajectory for a distance of 3.5 or 5.4 Å (black lines).

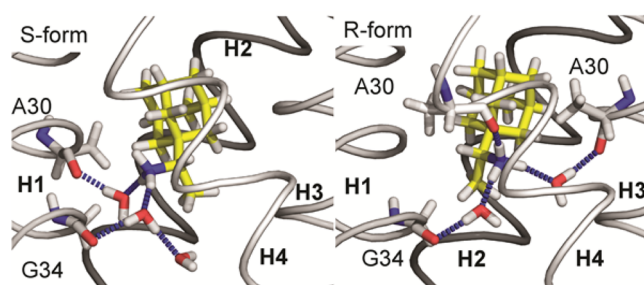


Figure 3. Representative structures of rimantadine (yellow) in a hydrogen-bonding network with the M2 channel and from NMR restrained RosettaLigand calculations followed by MD simulations.

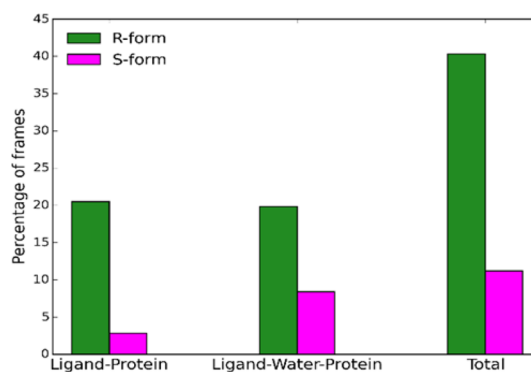


Figure 4. Comparison of hydrogen-bonding network between the (*R*)- and (*S*)- forms of rimantadine with M2. Ligand-Protein denotes the formation of direct hydrogen bonds between rimantadine and M2. Ligand-Water-Protein denotes the formation of water-mediated hydrogen bonds between rimantadine and M2. The y -axis of the plot denotes the percentage of simulation frames in which specific hydrogen-bonding types are present.

Figure 3, illustrating that the polar amine group of (*R*)-rimantadine is interacting with three hydrogen-bond acceptors

from three different monomers of M2 at the same time. One direct hydrogen bond is formed with the Ala30 backbone carbonyl; this carbonyl is in the same peptide plane as the Ser31 amide, which has a significantly perturbed ^{15}N chemical shift in the presence of rimantadine. In addition, two water-mediated hydrogen bonds are formed with the Ala30 and Gly34 carbonyls in two other monomers. In contrast, (S)-rimantadine only infrequently forms direct hydrogen bonds and only half as frequently forms water-mediated hydrogen bonds with Ala30 and Gly34 (Figure 4). The result is a reduced stability for the (S)- enantiomer, as shown by partial occupancy of the binding site in Figure 1, while the (R)- enantiomer is exhibiting full occupation.

Despite the four-fold symmetry of the drug binding site, the interactions with a chiral ligand are very different, suggesting that the (R)-enantiomer is the more effective drug. More importantly, the observation of chiral interactions with a four-fold symmetric structure is important for future drug design efforts. The complex set of interactions that are mediated by the (R) enantiomer involving three of the helices suggests that complex structural rearrangements are needed, as these interactions involve all four helices to generate the NMR-observed time-averaged structure. Together these results deepen our understanding of the atomic-level interactions stabilizing inhibitors in the M2 channel pore.

■ ASSOCIATED CONTENT

Supporting Information

The Supporting Information is available free of charge on the ACS Publications website at DOI: 10.1021/jacs.5b13129.

Experimental procedures, spectroscopic data, and data tables (PDF)

■ AUTHOR INFORMATION

Corresponding Author

*cross@magnet.fsu.edu

Notes

The authors declare no competing financial interest.

■ ACKNOWLEDGMENTS

We thank Dr. Huajun Qin for assistance with cloning of the M2 protein. Dr. Zhehong Gan, Dr. Bill Brey, and Peter Gor'kov from the NHMFL assisted with the NMR experiments and NMR probe technology. This work was supported in part by the National Institutes of Health R01AI023007 and P01AI074805 and conducted at the National High Magnetic Field Laboratory supported by NSF DMR-1157490 and the State of Florida. G.B.D. gratefully acknowledges the support of the National Science Foundation (CHE-1300722).

■ REFERENCES

- (1) *Code of Federal Regulations 21:1308*; U.S. Government Printing Office: Washington, DC, 1995.
- (2) Andreas, L. B.; Barnes, A. B.; Corzilius, B.; Chou, J. J.; Miller, E. A.; Caporini, M.; Rosay, M.; Griffin, R. G. *Biochemistry* **2013**, *52*, 2774–82.
- (3) McMenamy, R. H.; Oncley, J. L. *J. Biol. Chem.* **1958**, *233*, 1436–1447.
- (4) Takeda, M.; Pekosz, A.; Shuck, K.; Pinto, L. H.; Lamb, R. A. *J. Virol* **2002**, *76*, 1391–1399.
- (5) Li, C.; Qin, H.; Gao, F. P.; Cross, T. A. *Biochim. Biophys. Acta, Biomembr.* **2007**, *1768*, 3162–3170.
- (6) Schnell, J. R.; Chou, J. J. *Nature* **2008**, *451*, 591–595.

(7) Cady, S. D.; Schmidt-Rohr, K.; Wang, J.; Soto, C. S.; Degrado, W. F.; Hong, M. *Nature* **2010**, *463*, 689–692.

(8) (a) Sharma, M.; Yi, M.; Dong, H.; Qin, H.; Peterson, E.; Busath, D. D.; Zhou, H. X.; Cross, T. A. *Science* **2010**, *330*, 509–512. (b) Acharya, R.; Carnevale, V.; Fiorin, G.; Levine, B. G.; Polishchuk, A. L.; Balannik, V.; Samish, I.; Lamb, R. A.; Pinto, L. H.; DeGrado, W. F.; Klein, M. L. *Proc. Natl. Acad. Sci. U. S. A.* **2010**, *107*, 15075–15080.

(9) Stouffer, A. L.; Acharya, R.; Salom, D.; Levine, A. S.; Di Costanzo, L.; Soto, C. S.; Tereshko, V.; Nanda, V.; Stayrook, S.; DeGrado, W. F. *Nature* **2008**, *451*, 596–599.

(10) Can, T. V.; Sharma, M.; Hung, I.; Gor'kov, P. L.; Brey, W. W.; Cross, T. A. *J. Am. Chem. Soc.* **2012**, *134*, 9022–9025.

(11) Hu, J.; Asbury, T.; Achuthan, S.; Li, C.; Bertram, R.; Quine, J. R.; Fu, R.; Cross, T. A. *Biophys. J.* **2007**, *92*, 4335–4343.

(12) Cady, S. D.; Wang, J.; Wu, Y.; DeGrado, W. F.; Hong, M. *J. Am. Chem. Soc.* **2011**, *133*, 4274–4284.

(13) Andreas, L. B.; Eddy, M. T.; Pielak, R. M.; Chou, J.; Griffin, R. G. *J. Am. Chem. Soc.* **2010**, *132*, 10958–10960.

(14) (a) Dolin, R.; Reichman, R. C.; Madore, H. P.; Maynard, R.; Linton, P. N.; Webber-Jones, J. N. *Engl. J. Med.* **1982**, *307*, 580–584.

(b) Hay, A. J.; Wolstenholme, A. J.; Skehel, J. J.; Smith, M. H. *EMBO J.* **1985**, *4*, 3021–3024. (c) Wang, C.; Takeuchi, K.; Pinto, L. H.; Lamb, R. A. *J. Virol.* **1993**, *67*, 5585–5594. (d) Kukol, A.; Adams, P. D.; Rice, L. M.; Brunger, A. T.; Arkin, T. I. *J. Mol. Biol.* **1999**, *286*, 951–962. (e) Wang, J.; Kim, S.; Kovacs, F.; Cross, T. A. *Protein Sci.* **2001**, *10*, 2241–2250.

(15) Nishimura, K.; Kim, S.; Zhang, L.; Cross, T. A. *Biochemistry* **2002**, *41*, 13170–13177.

(16) Furuse, Y.; Suzuki, A.; Oshitani, H. *Antimicrob. Agents Chemother.* **2009**, *53*, 4457–4463.

(17) Dong, G.; Peng, C.; Luo, J.; Wang, C.; Han, L.; Wu, B.; Ji, G.; He, H. *PLoS One* **2015**, *10*, e0119115.

(18) (a) Hay, A. J. *Semin. Virol.* **1992**, *3*, 21–31. (b) Sansom, M. S.; Kerr, I. D. *Protein Eng., Des. Sel.* **1993**, *6*, 65–75.

(19) Yi, M.; Cross, T. A.; Zhou, H. X. *J. Phys. Chem. B* **2008**, *112*, 7977–7979.

(20) Balannik, V.; Wang, J.; Ohigashi, Y.; Jing, X.; Magavern, E.; Lamb, R. A.; Degrado, W. F.; Pinto, L. H. *Biochemistry* **2009**, *48*, 11872–1182.

(21) Tanuwidjaja, J.; Peltier, H. M.; Ellman, J. A. *J. Org. Chem.* **2007**, *72*, 626–629.

(22) Davis, I. W.; Baker, D. *J. Mol. Biol.* **2009**, *385*, 381–392.